#33

Papers from the GEOPHYSICAL LABORATORY
Carnegie Institution of Washington
No. 1752

Proc. Lunar Planet. Sci. Conf. 9th (1978), p. 2919–2934.
Printed in the United States of America

Effects of compositional variation on absorption spectra of lunar pyroxenes

R. M. HAZEN, P. M. BELL, and H. K. MAO

Geophysical Laboratory, Carnegie Institution of Washington, Washington, D.C. 20008

Abstract—Polarized absorption spectra of lunar pyroxenes with a range of iron, calcium, magnesium, titanium, and chromium contents were measured on polished, oriented single crystals. Spectral data on pure synthetic orthoferrosilite, $FeSiO_3$, are also recorded. Peaks at 2 μm, 1 μm, 550, 505, 460–480, and 430 nm are present in $FeSiO_3$ and are assigned to crystal-field transitions of Fe^{2+} in octahedral coordination because it is the only transition element present. The bands at 1 and 2 μm vary significantly in position with composition within the pyroxene quadrilateral; wavelengths increase with increasing calcium and iron. The energy represented by the separation between these two bands increases with Fs content for low-calcium pyroxenes, but decreases with Wo content, essentially independent of iron, for augites.

In the visible region, a weak band at 640 nm correlates in intensity with Cr_2O_3, but not with titanium as had been previously suggested. The 505 nm ferrous iron peak is a sharp doublet in most low-calcium pyroxenes, but a singlet in augites. This difference is ascribed to splitting in $P2_1/c$ and *Pbca* pyroxenes of a peak that is a singlet in $C2/c$ pyroxenes. A peak at 475 nm and an intense absorption edge below 700 nm correlate with titanium content. These data should aid in the interpretation of diffuse reflectance spectra of remote objects.

INTRODUCTION

Spin-allowed crystal-field absorption bands of pyroxenes dominate visible and near-infrared reflectance spectra of lunar materials (Adams and McCord, 1972; Adams, 1974, 1975). The positions and intensities of pyroxene absorption features are sensitive to composition, and observed variations in reflectance spectra may, therefore, be related to average pyroxene composition.

Interpretation of diffuse reflectance spectra must be based, in part, on correlations between composition and absorption spectra of minerals. Important features of single-crystal polarized absorption spectra of lunar and terrestrial pyroxenes have been reported by numerous investigators (see e.g., Burns, 1970; Burns *et al.*, 1972a,b; Mao and Bell, 1973; Runciman *et al.*, 1973; Adams *et al.*, 1973; Burns and Vaughan, 1975; Sung *et al.*, 1977). Although these authors have noted variations in spectra for pyroxenes with different iron, calcium, titanium, and chromium content, the quantitative nature of these changes has not been completely documented. Controversy still exists over the assignment of several absorption features in the visible region of pyroxene spectra. Furthermore, little attention has been devoted to the effects of zoning, exsolution, and ordering on the spectra of lunar and terrestrial pyroxenes.

Hazen *et al.* (1977) have demonstrated that a systematic study of spectral variation over a wide range of mineral compositions may aid in the interpretation of the mineral's absorption phenomena. This systematic approach is especially relevant to the study of lunar pyroxenes, which are highly variable in both essential and minor element compositions. The principal objectives of this study are

(1) to quantify some changes in lunar pyroxene absorption spectra due to variations in composition,
(2) to suggest possible spectral variations due to zoning and exsolution,
(3) to define absorption features that might contribute to diffuse reflectance spectra of pyroxene-bearing materials.

EXPERIMENTAL

Single crystals of pyroxene, from 150 to 650 μm in maximum dimension, were selected from lunar soils and rock fragments. Eleven crystals were optically oriented, mounted in epoxy, and polished on both parallel sides to a thickness of 25 to 220 μm. In addition, four pyroxenes from Luna 24 sample 182,48 were selected from polished grain mounts. Pyroxenes were chemically analyzed at three to seven points (depending on degree of zoning and size of grain) with an automated electron microprobe. Averaged analyses are presented in Table 1 and illustrated on the pyroxene quadrilateral in Fig. 1, with data for twenty pyroxenes described in previous studies. Orthopyroxenes and pigeonites are compositionally uniform. Several of the augites, however, are zoned or have exsolved pigeonites, as noted in Table 1. Polarized spectra of fifteen pyroxenes were measured using techniques described by Mao and Bell (1973). After measurement of those pyroxenes from Apollo 12 and 17 samples, grains were removed from the epoxy and crystal thicknesses were measured. The four thickest grains were remounted and repolished at 90° to the original orientation, to obtain complete α, β, and γ spectra for those pyroxenes.

Data are also presented on the 400 to 700 nm polarized spectra of pure synthetic orthoferrosilite, $FeSiO_3$. Orthoferrosilite was synthesized from an oxide mix in a piston cylinder apparatus at 1000°C and 25 kbar for 10 hours. Near-infrared spectra of this material were reported by Mao and Bell (1971). Spectral data for 34 pyroxenes from this and previous studies are recorded in Table 2.

REVIEW OF PYROXENE ABSORPTION SPECTRA

Polarized absorption spectra for eight pyroxenes with different compositions are illustrated in Fig. 2. Major features present in all spectra are the 1 and 2 μm bands due primarily to spin-allowed *d-d* crystal-field (CF) transitions of Fe^{2+} in M2 based on calculations of transition energies (Burns, 1970; Runciman *et al.*, 1973). Also present in the near-infrared region of the γ spectrum is a weaker 1200 nm peak or shoulder due to a spin-allowed CF transition of Fe^{2+} in M1.

Below 700 nm, in the visible region, several small absorption features are observed (Fig. 3). Peaks at 550 and 507 nm, and a shoulder at 425 nm, are assigned to spin-forbidden CF transitions in Fe^{2+}, owing to their sharpness, low intensity, and presence in pyroxenes without titanium or chromium (Burns *et al.*, 1972a, 1973). Mao and Bell (1971) and Bell and Mao (1972), however, suggested that Fe^{3+} or Ti^{3+}-Ti^{4+} charge transfer (CT) might contribute to the 507 nm peak. Burns *et al.* (1976) assigned the weak bands at 475 and 650 nm to Ti^{3+} spin-allowed CF transitions in M1, on the basis of correlations with titanium content in both lunar and terrestrial pyroxenes. Other interpretations of the 650 nm peak include $Fe^{3+} \rightleftarrows Fe^{2+}$ CT transitions (Cohen, 1972) and Cr^{3+} CF transitions (Rossman, 1977).

The weak peaks below 700 nm are superimposed on a strong absorption edge that is probably due to complex metal-oxygen and metal-metal CT effects (Loeffler *et al.*, 1974). In addition to the features noted above, which are also the major bands observed in this study, Burns *et al.* (1973) documented weak bands at 450 and 600 nm in a zoned pyroxene from specimen 15058 with high Cr^{3+}/Fe^{2+}, and very weak peaks at 400 and 585 nm in several lunar pyroxenes. The 450 and 600 nm peaks, which are assigned to chromium, are similar to Cr^{3+} bands in other minerals, and the 400 and 585 nm peaks are assigned to spin-forbidden CF transitions of Fe^{2+} on the basis of their sharpness and low intensity.

Table 1. Pyroxene compositions (see also Fig. 1)*

No.	Specimen	No. of points	SiO_2	Al_2O_3	MgO	FeO	CaO	MnO	Cr_2O_3	TiO_2	Total	Reference
1	7324-3	7	53.0	0.79	24.0	18.8	1.99	0.38	0.62	0.74	100.4	This study
2	12033-4	6	53.0	1.60	22.2	17.2	4.72	0.37	0.85	0.70	100.6	This study
3	12041-2	4	53.5	0.94	24.3	16.5	3.74	0.37	0.60	0.41	100.4	This study
4	12040-2	3	50.3	0.84	17.5	24.3	5.54	0.44	0.27	0.70	99.9	This study
5†	L24-182,3	5	51.2	1.18	16.1	22.9	7.70	0.41	0.56	0.24	100.2	This study
6	73261-3	6	50.6	2.16	19.6	15.9	8.32	0.38	0.68	1.60	99.3	This study
7‡	73241-1	5	52.0	1.75	15.9	13.6	15.2	0.32	0.80	0.84	100.5	This study
8	12033-2	3	48.9	4.47	14.2	13.7	14.7	0.29	1.29	1.51	99.2	This study
9‡	73261-4	5	51.3	1.14	14.0	15.3	16.1	0.36	0.11	1.10	99.4	This study
10†	70017-1	5	50.2	1.87	14.7	19.1	11.8	0.39	0.52	1.41	100.0	This study
11	12001-1	3	49.1	2.18	14.2	19.3	12.6	0.36	0.42	1.61	99.8	This study
12†	L24-182,1	5	51.5	1.63	13.8	20.8	11.3	0.40	0.52	0.37	100.3	This study
13	73261-1	5	48.3	1.47	10.0	22.4	14.4	0.44	0.65	0.89	98.8	This study
14†	L24-182,4	5	49.1	1.10	9.6	29.3	9.27	0.52	0.23	0.41	99.5	This study
15	L24-182,2	5	47.9	1.12	4.5	28.8	16.5	0.44	0.10	1.02	100.4	This study
16§	Kimberley-Enstatite		57.68	0.82	35.84	4.63	0.36	<0.05	0.22	<0.05		Runciman *et al.* (1973)
17§	Norway-Bronzite		58.8	—‖	31.64	9.56	—	—	—	—		Bancroft and Burns (1967)
17a§	Norway-Bronzite		57.83	0.09	32.86	9.77	0.26	—	—	—		Goldman and Rossman (1977)
18§	Manchuria Opx		46.0	0.90	3.49	41.7	1.43	5.02	—	0.10		Burns (1970)
19§	Synthetic $FeSiO_3$		47.1	0.0	0.0	52.9	0.0	0.0	0.0	0.0		Mao and Bell (1971)
20	Cr-diopside		55.34	1.32	19.49	2.39	17.94	—	1.49	0.04		Mao *et al.* (1972)
21	Quebec-Hedenbergite		49.0	0.3	1.8	25.78¶	22.0	0.44	—	0.0		Burns *et al.* (1972a)
22§	L22002-2,4d		56.10	1.36	29.87	11.93	1.43	0.24	0.73	0.22		Adams *et al.* (1973)
23	12040,49		52.55	1.27	23.63	15.75	3.85	0.32	—	0.52		Bell and Mao (1972)
24	14306,6		54.15	0.90	23.90	18.72	1.69	0.36	0.28	0.52		Bell and Mao (1972)
25	14053-Pig.		52.10	1.75	21.67	17.22	4.95	—	—	0.75		Bell and Mao (1972)
26	12021-Pig.		51.5	2.05	21.9	16.9	5.1	0.37	0.93	0.68		Burns *et al.* (1972b)
27	L20-A8		52.79	1.38	15.48	18.96	9.20	0.45	0.66	0.46		Adams *et al.* (1973)
28	14053-Augite		50.24	1.62	14.08	21.05	12.00	—	—	1.37		Bell and Mao (1972)
29A†	12063,79 } Pig.		51.15	2.01	18.70	16.37	7.98	0.35	0.70	1.20		Mao and Bell (1973)
29B†	12063,79 } Augite		50.00	3.34	15.09	11.89	15.25	0.27	0.94	1.93		Mao and Bell (1973)
30†	10047,70		49.37	2.07	15.41	14.01	15.49	0.27	0.39	1.99		Burns *et al.* (1976)
31†	L24-Inner		51.47	2.01	14.95	15.44	15.04	0.36	0.79	0.34		Rossman (1977)
32	74275,85		45.07	6.51	12.51	10.11	19.10	0.21	0.75	5.25		Burns *et al.* (1976)
33†	L24-Outer		48.30	1.03	6.60	31.02	12.22	0.42	0.09	0.92		Rossman (1977)
34†	12021-Augite		50.2	3.32	15.3	13.1	15.7	0.31	1.01	1.26		Burns *et al.* (1972b)

*NiO and Na_2O, when analyzed, in trace amounts only.
†Strongly zoned augite.
‡Augite with exsolved pigeonite.
§Orthopyroxene.
‖Not reported.
¶1.53% Fe_2O_3.

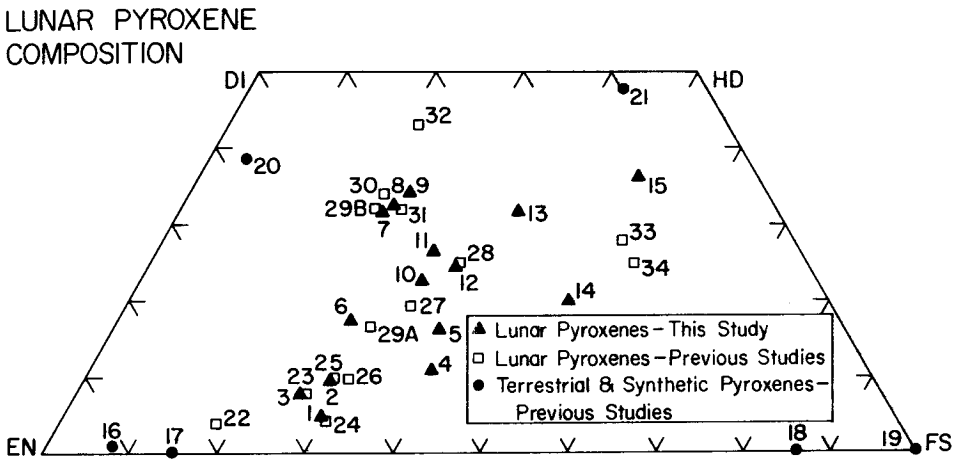

Fig. 1. Pyroxene compositions projected onto the $(Mg,Fe,Ca)SiO_3$ quadrilateral.

Although Mn^{2+} absorption effects are well documented in terrestrial chain silicates (Manning, 1968), it is generally assumed that the weak absorption due to the ≈0.4 wt. % MnO in most lunar pyroxenes is masked by iron and titanium (Burns and Vaughan, 1975). In addition, Mössbauer and spectral data suggest that iron and chromium are present almost completely as Fe^{2+} and Cr^{3+}, rather than Fe^{3+} and Cr^{2+}, in lunar pyroxenes (Burns *et al.*, 1973). Titanium, on the other hand, is present as both Ti^{3+} and Ti^{4+}, with $Ti^{3+}/Ti^{4+} \approx 0.6$–$0.7$ in some lunar pyroxenes (Sung *et al.*, 1974). The only cations of concern in describing lunar pyroxene spectra, therefore, are Fe^{2+}, Cr^{3+}, Ti^{3+}, and Ti^{4+}.

RESULTS

The spectrum of synthetic orthoferrosilite, $FeSiO_3$

The absorption spectrum of pure $FeSiO_3$ provides an important standard of comparison for natural pyroxene spectra. Ferrous iron is the only transition element in this material, and all spectral features are, therefore, unambiguously assigned to Fe^{2+} in either M1 or M2. The 1 and 2 μm features are well documented ferrous iron absorption effects in all measured pyroxene spectra (Burns, 1970). The 700 to 400 nm spectrum of orthoferrosilite (Fig. 3) establishes that peaks at 550, 508, 460–480, and 437 nm are also Fe^{2+} effects in the iron end-member pyroxene. Ferrous iron *alone* does not appear to contribute to absorption at 640, 585, or 450 nm observed in lunar pyroxenes. In natural pyroxenes, contributions from titanium and chromium CF effects, as well as metal-metal (Ti-Fe, Fe-Fe) CT will be superimposed on the ferrous iron absorption features.

The 2 μm band

Systematic variations in the positions of the 1 and 2 μm pyroxene absorption maxima with composition have been illustrated by several authors (Adams and

Table 2. Spectral data for pyroxenes

No.	Specimen	Orientation	1 μm Band Intensity-β λ (nm)	1 μm Band Intensity-β (cm⁻¹)	2μm Band Intensity-β λ (nm)	2μm Band Intensity-β (cm⁻¹)	β I(1 μm/2 μm)	Energy Δ* 1 μm − 2 μm (cm⁻¹)	Slope of absorption edge†	Nature of 505 nm peak	Other features‡ 425	470	550	640
1	73241-3	α-β-γ	925	400	1930	70	5.7	5630	5	506 singlet	m	m	m	1.5
2	12033-4	α-β-γ	930	250	1900	80	3.1	5490	14	504 & 507 doublet	w	m	m	2.0
3	12041-2	α-β	925	225	1890	60	3.8	5520	5	503 & 507 doublet	m	m	m	2.5
4	12040-2	α-β-γ§	935	475	1950	80	5.9	5570	12	503 & 507 doublet	m	m	s	0.5
5	L24-182,3	≈β-≈γ‖	940	—¶	—	—	—	—	—	507 singlet	a	s	m	1.0
6	73261-3	β-γ	940	550	2000	—	—	5640	44	504 & 507 doublet	w	m	w	1.5
7	73241-1	α-β-γ§	980	450	2130	150	3.0	5510	23	506 singlet	s	s	m	3.0
8	12033-2	α-γ	1000	—	2150	—	—	5350	50	503 & 506 broad	s	s	w	7.0
9	73261-4	α-γ	965	—	2120	—	—	—	29	508 singlet	w	m	m	0
10	70017-1	β-γ	955	450	—	—	—	—	23	506 singlet	a	a	s	2.0
11	12001-1	β-γ	980	600	2040	—	—	5300	36	506.5 singlet	m	s	w	0.5
12	L24-182,1	≈α-≈γ‖	955	—	—	—	—	—	—	508 singlet	a	m	m	1.0
13	73261-1	β-γ	990	550	2150	—	—	5450	38	507.5 singlet	a	s	m	1.0
14	L24-182,4	≈β-≈γ‖	950	—	2050	—	—	5650	—	508 singlet	s	s	s	1.0
15	L24-182,2	≈β-≈γ‖§	1010	—	2220	—	—	5400	—	510 singlet	a	s	s	1.0
16	Kimberley-Enstatite	α-β-γ	920	>>20	1850	20	>5	5460	1	505 broad	m	m	w	m
17	Norway-Bronzite	α-β-γ	920	—	1860	—	3.9	5490	—	504 & 507 doublet	—	vw	s	a
17a	Norway-Bronzite	α-β-γ	920	—	1860	—	—	5490	—	Doublet	w	m	s	a
18	Manchuria Opx	α-β-γ	935	—	2040	—	1.4	5790	—	508 singlet	m	s	s	s
19	Synthetic $FeSiO_3$	α-γ	935	—	—	—	—	—	—	—	s	s	s	a
20	Cr-diopside	α-β-γ	1020	35	—	—	—	—	—	—	a	vs	a	≈10
21	Quebec-Hedenbergite	α-β-γ	1040	—	2250	—	4.5	5170	—	≈505 singlet	vw	vw	s	a
22	L22002-2,4d	α-β-γ§	925	100	1870	45	2.2	5460	10	—	a	m	a	a
23	12040,49	β-γ	930	—	1900	—	—	5490	—	503 & 507 doublet	m	w	s	s
24	14306,6	α-β-γ	925	80	1900	55	1.5	5550	5	≈505	m	vw	s	m
25	14053-Pigeonite	α-β-γ§	930	240	1900	60	4.0	5490	9	504 & 507 doublet	s	m	m	s
26	12021-Pigeonite	α-β-γ	930	—	—	—	—	—	—	≈505 broad	m	a	m	a
27	L20-A8	α-β-γ§	945	—	2000	—	2.8	5580	—	—	m	m	m	s
28	14053-Augite	α-β-γ	955	280	2015	45	6.2	5510	30	≈505 singlet	s	w	m	m
29	12063,79	α-β-γ	965	—	2250	—	1.4	5920	—	≈505 broad	w	m	m	m
30	10047,70	α-β-γ	1015	—	2150	—	7	5200	—	≈505 broad	m	m	m	m
31	L24-Inner	≈α + β‖	970	—	—	—	—	—	—	—	a	a	w	vw
32	74275,85	α-β-γ§	1020	—	2200	—	6	5260	≈200**	≈505 broad	a	vs	s	a
33	L24-Outer	≈α + β‖	970	—	2100	—	—	5550	—	—	a	a	w	w
34	12021-Augite	α-β-γ§	975	—	2100	—	1.4	5490	—	≈505 sharp	m	a	m	w

*$\Delta E = (1/\lambda_1 - 1/\lambda_2)$.
†Difference of absorption coefficients at 500 and 700 nm.
‡a – absent, vw – very weak, w – weak, m – moderate, s – strong, vs. – very strong.
§Illustrated in Fig. 2.
‖Spectra taken from polished section.
¶Data not available.
**Based on assumed 1 μm band intensity of ≈350.

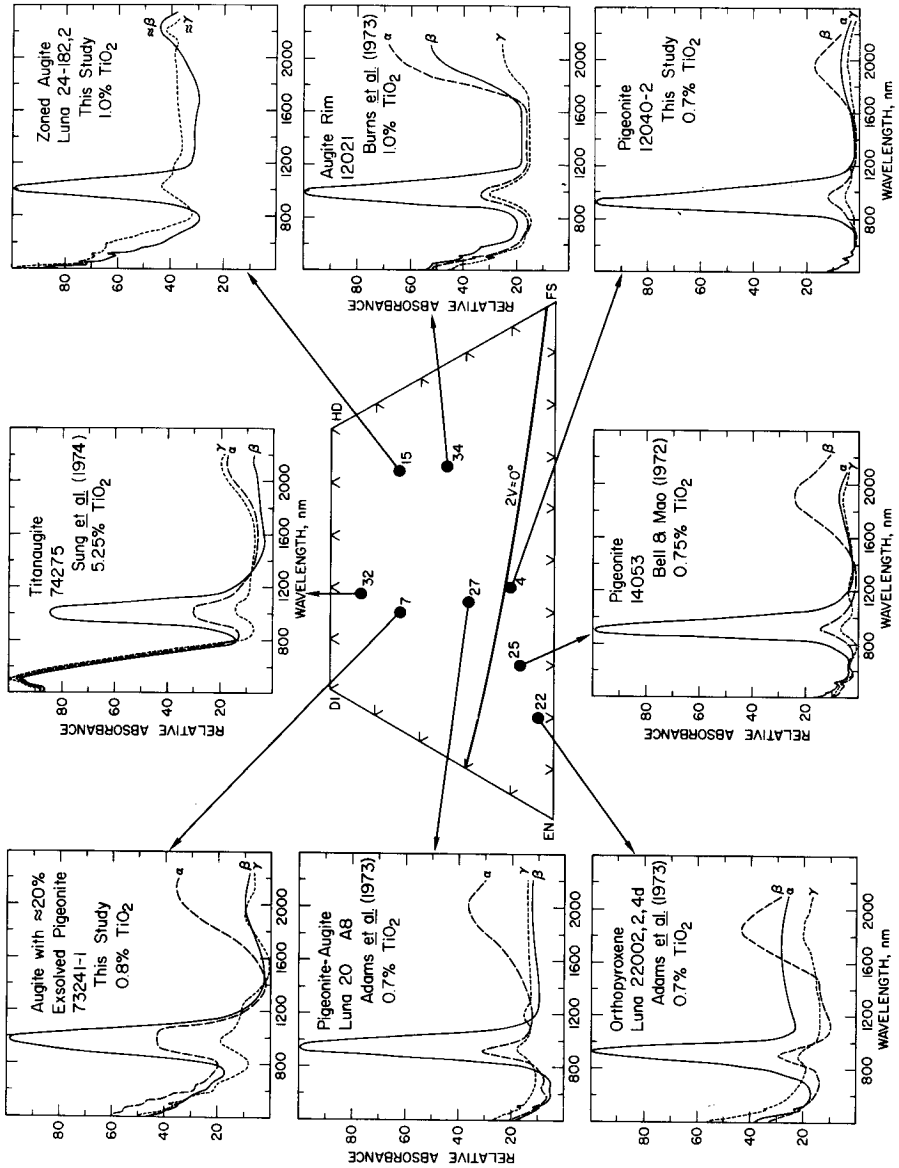

Fig. 2. Absorption spectra of eight lunar pyroxenes.

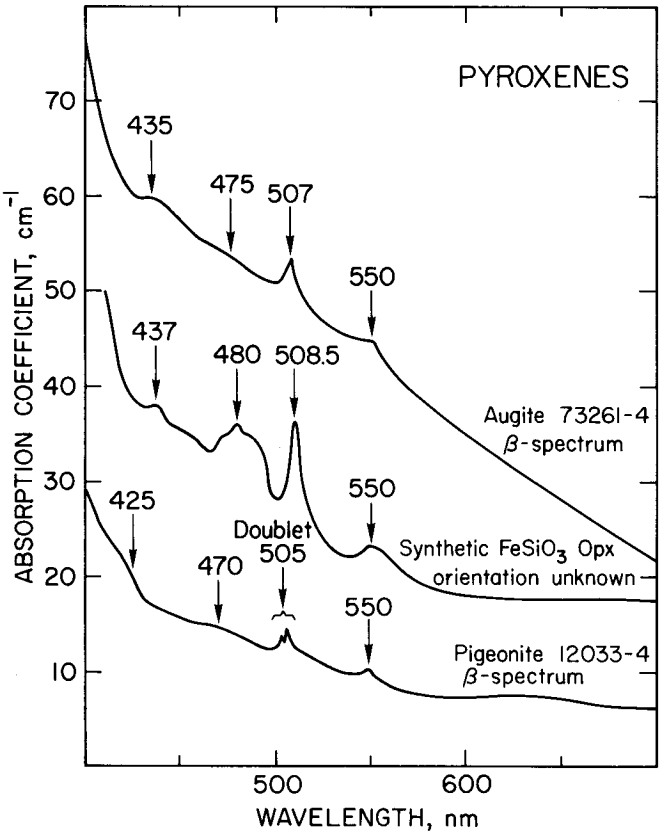

Fig. 3. Visible region absorption spectra of lunar pigeonite 12033-4, lunar augite 73261-4, and synthetic $FeSiO_3$.

McCord, 1972; Adams, 1974; Sung *et al.*, 1977). The details of these variations on the pyroxene quadrilateral, however, have not been presented previously, and are illustrated in Figs. 4 and 5. The energy represented by the 2 μm band, which is due to spin-allowed CF transitions of Fe^{2+} in M2, decreases with increasing iron and calcium content. The addition of calcium and iron to enstatite increases the size and alters the distortion of the M2 site, thus lowering the transition energy.

The positions of the 2 μm maxima observed for lunar and terrestrial orthopyroxenes and pigeonites are generally within 10 nm of the values plotted in Fig. 4. In augites, which frequently have compositional zoning, 2 μm peaks deviate by less than 30 nm of plotted values except for three specimens, of which 73241-1 has coarsely exsolved pigeonite and 12063,79 and 10047,70 are strongly zoned. These pyroxenes, all of which show 2 μm peak positions at wavelengths longer than expected for their compositions, have regions of higher than average (Fe + Ca) in M2. These high Fe-Ca portions of the crystals contribute more to absorption than low Fe-Ca portions, and thus zoning or exsolution causes the shift of the band to

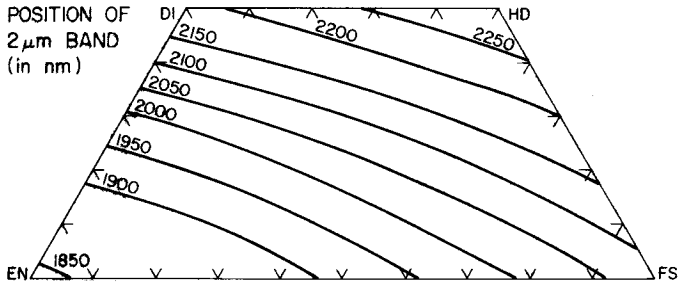

Fig. 4. Position of the 2 μm pyroxene absorption maxima vs. composition, projected on the pyroxene quadrilateral.

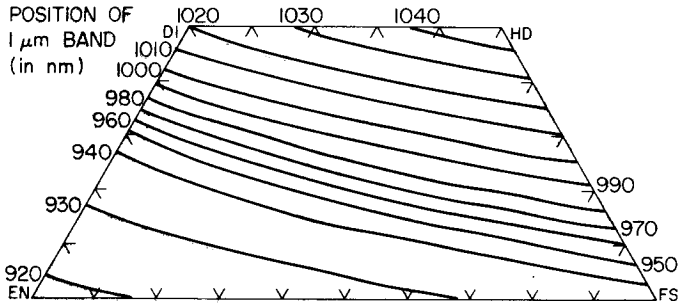

Fig. 5. Position of the 1 μm pyroxene absorption maxima vs. composition, projected on the quadrilateral.

longer wavelength. It should be noted that because there is no Fe^{2+} in M2 sites of ideal Ca-end member clinopyroxenes, the 2 μm band should not be observed for pyroxenes on the DI-HD join.

The 1 μm band

The positional variation vs. composition of the 1 μm band is illustrated in Fig. 5. The general trends of this plot are very similar to those of Fig. 4, and the same explanation is proposed. Positions for orthopyroxenes and pigeonites agree with the plotted values within 2 nm, whereas those for compositionally uniform augites differ by less than 10 nm. Zoned augites and those with exsolved pigeonite deviate by as much as 20 nm from the values of Fig. 5. The largest deviation from the trends outlined in Fig. 5 is for a terrestrial Cr-diopside. It is possible, therefore, that pyroxenes with high Cr/Fe will not conform to this plot.

Separation of the 1 and 2 μm bands

In an octahedral environment, ferrous iron (d^6 configuration) has three lower energy (t_{2g}) and two higher energy (e_g) levels. In a distorted environment these

degenerate levels are further split, and the energies of splitting provide information about the electronic structure of the Fe^{2+} cation. In pyroxenes the 1 μm band is a result of the transition from the lowest t_{2g} level to the higher e_g level, whereas the 2 μm band is due to the transition from the lowest t_{2g} level to the lower e_g level (Goldman and Rossman, 1977). The energy between the 1 and 2 μm bands is, therefore, equal to the splitting energy of the two e_g levels of Fe^{2+} in the distorted M2 site.

The energy of separation between the 1 and 2 μm bands of pyroxenes has been calculated directly from empirical information in Figs. 4 and 5, and is illustrated in Fig. 6. A line of inflection, which is very close to the $2V = 0°$ line for pyroxenes, divides the pyroxene quadrilateral into two distinct regions. Low-calcium pyroxenes (below $\approx Wo_{10}$) have 1–2 μm separation energies that are primarily a function of iron content. Pigeonites and orthopyroxenes with a content less than Fs_{40} show little variation in splitting energy, but between Fs_{40} and Fs_{100} the separation energy increases by 7%. Augites display a strikingly different trend in e_g splitting, with separation energy primarily a function of calcium content. The splitting energy decreases by approximately 8% between Wo_{15} and Wo_{50}, owing to the larger and more regular environment for iron in a calcium-rich M2 site.

Intensities of the 1 and 2 μm bands

The intensities of the 1 and 2 μm bands (see Table 2) appear to be complex functions of composition, zoning, exsolution, and ordering. In general, maximum absorption is greater for augites than for pigeonites or orthopyroxenes, and iron-rich pyroxenes show greater absorption than pyroxenes near the diopside-enstatite join. Goldman (1977) has demonstrated that the intensity of absorption due to iron in M1 is significantly less than for iron in M2, and it is probable that the absorption efficiency of these octahedral sites will also vary with composition.

The ratio of intensities, I(1 μm/2 μm), varies from less than 2 to about 7 for the pyroxenes studied. This ratio will be affected by several factors, including zoning, ordering, exsolution, and calcium and iron content. Zoning and exsolution will affect the peak heights by broadening. Ordering of Fe and Mg causes significant

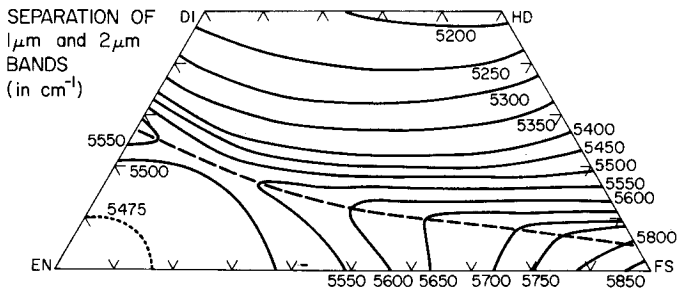

Fig. 6. Difference in energy between the 1 and 2 μm bands. This difference is related to the distortion of the M2 octahedral site.

changes in peak-height ratios because the 1 μm band includes some contributions from iron in M1, whereas the 2 μm band is due entirely to iron in M2 (Burns, 1970; Runciman *et al.*, 1973; Goldman, 1977). Calcium and iron content affect the peak-height ratio because all calcium must enter the M2 site. For pyroxenes with a content greater than Wo_{40} and Fs_{10}, significant amounts of iron must enter the M1 site. Pyroxenes near hedenbergite, therefore, may have greater than average I(1 μm/2 μm).

Goldman and Rossman (1977) have noted that intensities of absorption measured with microscope spectrophotometers, as used in this study, may be in error owing to mixing of polarization components in the strongly convergent light of the optical system. This mixing may cause peak broadening (as in Fig. 2, augite 73241-1 α spectrum 1 μm peak; 74275 titanaugite), which in turn may lead to erroneous peak-intensity measurements. The absolute and relative intensities reported in this study must, therefore, be considered qualitatively, but not necessarily quantitatively, correct.

The 640 nm peak

Confusion has arisen over the origin of the broad, weak band centered at about 640 nm. From heating experiments, Cohen (1972) assigned this feature to Fe^{3+}-Fe^{2+} CT in both terrestrial and lunar pyroxenes. Burns *et al.* (1972a, 1973, 1976) attributed a 660 nm band to Ti^{3+} CF spin-allowed transition and a 670 nm band to Ti^{3+}-Ti^{4+} CT, consistent with the absence of these effects in pyroxenes without titanium and the calculated energies of titanium transitions. Bell and Mao (1972) observed a very strong 640 nm peak in natural chromium diopside, and Rossman (1977) adopted this Cr^{3+} assignment for a 640 nm peak in a Luna 24 pyroxene, on the basis of his studies of Cr-bearing pyroxenes.

Intensity data in Table 2 suggest that the broad 640 nm feature is primarily a chromium effect in lunar pyroxenes. This trend is illustrated in Fig. 7, which shows a distinct correlation between peak intensity and weight percentage of Cr_2O_3. The effects of varying Cr^{3+} on the 640 nm region are especially dramatic for three pyroxenes with similar bulk composition ($\approx En_{43}Fs_{24}Wo_{33}$) but different Cr^{3+}, as illustrated in Fig. 8. The 640 nm feature is absent for pyroxene 73261-4 with 0.1% Cr_2O_3 (1.1% TiO_2), moderately strong for 73241-1 with 0.8% Cr_2O_3 (0.8% TiO_2), and strong for 12033-2 with 1.3% Cr_2O_3 (1.5% TiO_2).

There is no evidence for an observable titanium contribution to the 640 nm band. The lack of correlation between band intensity and total titanium, calculated as TiO_2, is illustrated in Fig. 7. It is concluded that, although there may be theoretical justification for a Ti^{3+} feature near 640 nm, these effects cannot be detected in most lunar pyroxenes by current techniques when Cr^{3+} is present.

The 505 nm peak

The most prominent feature in the visible region of pyroxene spectra is the sharp peak at 505 nm. Although considerable debate has occurred over the origin of

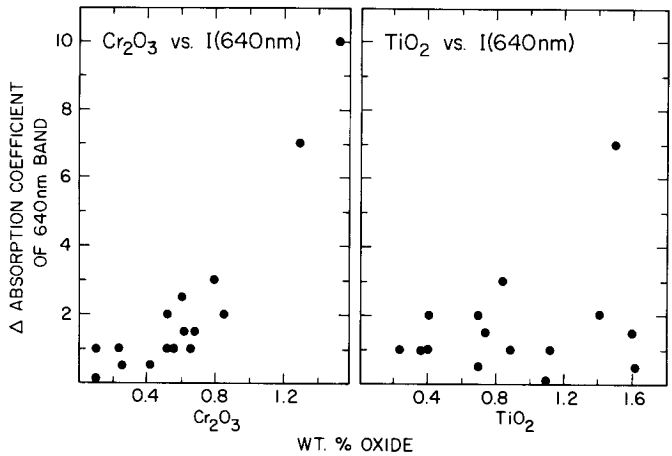

Fig. 7. Chromium and titanium content vs. Δ absorption coefficient of the 640 nm band. The Δ absorption coefficient is calculated by subtracting the 590–690 nm background and measuring the maximum band intensity.

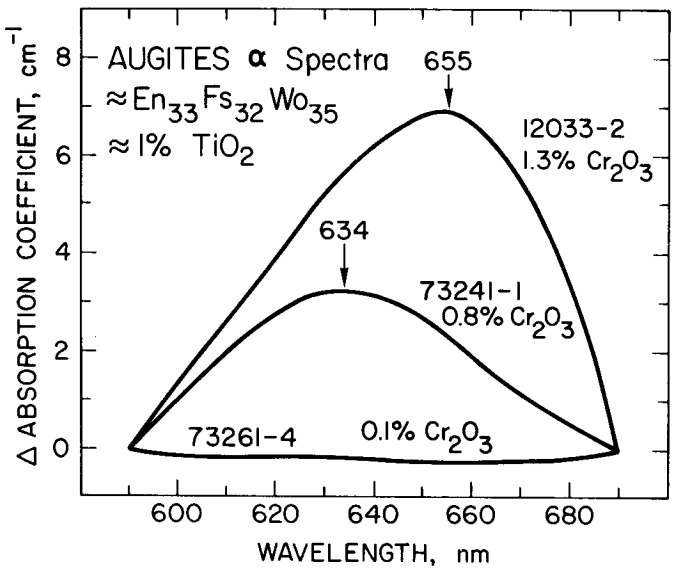

Fig. 8. Alpha spectrum peak at 640 nm vs. Δ absorption coefficient for pyroxenes with similar projected compositions, but differing chromium. The absorption coefficient is calculated by subtracting the 590–690 nm background. Therefore, intensities at 590 and 690 nm are set to zero.

this peak (Burns *et al.*, 1973), there is now general agreement with Burns *et al.* that the feature is a result of spin-forbidden CF transitions in six-coordinated Fe^{2+}. Data on orthoferrosilite (Fig. 3) support this assignment. The peak is clearly shown

as a doublet (≈503 and 507 nm) in several pigeonite spectra (Mao and Bell, 1971; Bell and Mao, 1972; Burns *et al.*, 1973), but it appears as a singlet in other pyroxenes. Burns *et al.* (1973) proposed that the doublet corresponds to a contribution from M1 at 503 nm and a contribution from M2 at 508 nm superimposed. They also suggested that the peak height ratios of the doublet might provide a sensitive index of ordering. Data on pure $FeSiO_3$ (Fig. 3 and Table 2) do not support this conclusion. The spectrum of ferrosilite has a single sharp peak at 508.5 nm, even though all of M1 and M2 are occupied Fe^{2+}. Furthermore, in a natural hedenbergite reported by Burns (1970) with the composition $En_9Fs_{48}Wo_{42}$, more than 80% of the iron must be in M1, because Ca is only in M2. The spectrum of hedenbergite, however, shows a single maximum at approximately 508 nm, rather than a doublet with maximum intensity at 503 nm as predicted by the Burns *et al.* model.

The nature of the 505 nm peak is illustrated on the pyroxene quadrilateral in Fig. 9. A striking aspect of this plot is that virtually all pigeonites and orthopyroxenes have a doublet or broad (4 nm) maximum between 505 and 508 nm, whereas high-calcium pyroxenes show sharp singlets for most specimens. The only exceptions to this trend are two iron-rich orthopyroxenes that show only singlets at 508 nm, and lunar augites 12033-2; 12063,79; 10047,70; and 74275,85 that show broad (3 nm wide) maxima rather than sharp peaks. No doublets are observed in the augite field.

A significant difference between high-calcium ($C2/c$) and low-calcium ($P2_1/c$) pigeonites and ($Pbca$) orthopyroxenes is the symmetry of the M1 site. There are no symmetry constraints on the M1 site of pigeonites and orthopyroxenes, whereas the M1 site of $C2/c$ clinopyroxenes has 2-fold symmetry. It is possible that the 505 nm feature is a result of spin-forbidden CF transitions of Fe^{2+} in M1, and that the splitting of this peak in pigeonites and some orthopyroxenes is due to the lower symmetry of that site. Further investigations of synthetic pyroxenes with differing degrees of order are needed to resolve the correct assignment of the 505 nm feature.

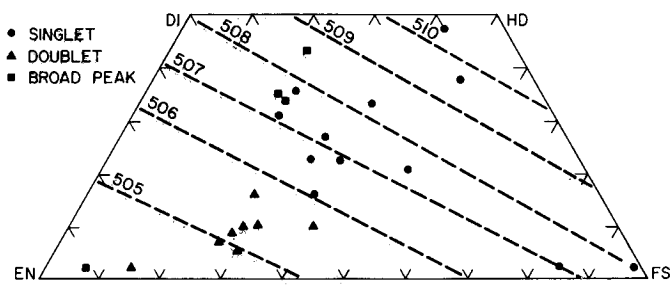

Fig. 9. Nature of the 505 nm pyroxene absorption peak. Symbols dot, triangle, and square stand for singlet, doublet, and broad peaks. Dashed lines represent variation of average peak position in nanometers.

The position of the 505 nm peak (or average position of doublets) varies regularly from less than 505 to greater than 510 nm over the pyroxene quadrilateral (Fig. 9). The contours plotted on Fig. 9 agree with observed data within 1 nm and are similar in trend to those for the positions of 1 and 2 μm bands (Figs. 4 and 5). No discontinuities are detectable across the augite/pigeonite/orthopyroxene fields for any of these peak positions. Because of the striking differences in 505 nm peak shape between *C*2/*c* and low-calcium pyroxenes, it is expected that additional data on pyroxenes between Wo_{10} and Wo_{25} may reveal small, but real, discontinuities in pyroxene spectral properties of these two structural variants.

The 425 and 550 nm peaks

Small peaks at 425 and 550 nm are ascribed to spin-forbidden CF transitions of Fe^{2+} by most authors. These peaks are present in pure synthetic $FeSiO_3$ (see Fig. 3) and are observed in most lunar pyroxene spectra (Burns *et al.*, 1973). The apparent intensity of these features is strongly dependent on the slope of the absorption edge below 600 nm.

The 470 nm peak

Burns *et al.* (1976, Fig. 4) demonstrated a strong correlation between the peak at 470 nm and TiO_2 content. Pyroxenes in this study with greater than 0.8% TiO_2 generally show strong 470 nm peaks as well. It should be noted, however, that pure $FeSiO_3$ also has a prominent band at about 475 nm (see Fig. 3), and a similar strong effect is observed in a natural iron-rich orthopyroxene (Burns, 1970). It must be concluded that the 470 nm feature is a superposition of Ti^{3+} and Fe^{2+} effects in lunar pyroxenes.

The absorption edge

Below 700 nm the pyroxene spectrum is dominated by an intense absorption edge, probably due to metal-metal and metal-oxygen CT effects. Calculations by Loeffler *et al.* (1974, 1975) indicate that the slope of the absorption edge below 700 nm will be primarily a function of titanium content, owing to Fe^{2+}-Ti^{4+} CT. Present observations also suggest that titanium has a dominant effect on the slope of the absorption edge. Pure $FeSiO_3$ (Fig. 3) has a relatively low slope between 500 and 700 nm, as measured by the differences in absorption coefficients between these two points. The slopes of lunar pyroxenes between 500 and 700 nm are well correlated with the weight percentage of TiO_2 (see Fig. 10). Scatter in these data should be reduced if Ti^{3+}/Ti^{4+} is known.

Conclusions

Data of this study support the belief that diffuse reflectance spectra may provide information on average pyroxene composition (Adams and McCord, 1972; Adams, 1974, 1975; Charette *et al.*, 1976, 1977). The major pyroxene absorption

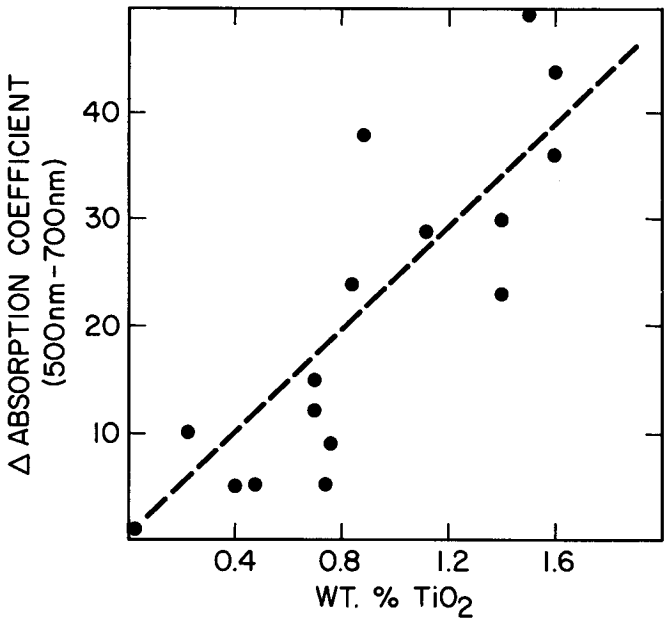

Fig. 10. Weight percentage of TiO_2 vs. slope of the absorption edge. The slope is calculated as the difference between absorption coefficients at 500 and 700 nm.

features, including the 2 and 1 μm bands and the absorption edge, are strongly dependent on variation of iron, calcium, magnesium, and titanium. Information on pyroxenes, combined with other systematic investigations of extraterrestrial materials (e.g., olivines, Hazen *et al.*, 1977; glasses, Mao *et al.*, 1978; pyroxenes at high temperature, Sung *et al.*, 1977) should provide a more quantitative basis for interpreting diffuse reflectance spectra of remote objects.

Controversy exists over the correct absorption spectra band assignments in many complex minerals. Much of the confusion and debate might be resolved by systematic studies of spectral variation with composition. In the pyroxene group, peaks at 2 μm, 1 μm, 550, 505, 460–480, and 430 nm are unambiguously assigned to Fe^{2+} in octahedral coordination on the basis of the spectrum of pure $FeSiO_3$. Other features in lunar pyroxene spectra may be attributed to titanium (the absorption edge and part of the 475 nm peak) and chromium (the 640 nm peak) on the basis of intensity vs. composition plots. In addition, effects due to zoning, exsolution, and structural state are observed in the spectra of pyroxenes.

Acknowledgments—The authors gratefully acknowledge the constructive comments and reviews of this manuscript by Roger G. Burns, George R. Rossman, Lucy McFadden, and Larry W. Finger. We thank the Carnegie Institution of Washington and NASA Grant NGL-09-140-012 for financial support of this research.

REFERENCES

Adams, J. B. (1974) Visible and near infrared diffuse reflectance spectra of pyroxenes as applied to remote sensing of solid objects in the solar system. *J. Geophys. Res.* **79,** 4829–4836.

Adams J. B. (1975) Interpretation of visible and near-infrared reflectance spectra of pyroxenes and other rock-forming minerals. In *Infrared and Raman Spectroscopy of Lunar and Terrestrial Minerals* (C. Karr, Jr., ed.), p. 90–116. Academic Press, N.Y.

Adams J. B., Bell P. M., Conel J. E., Mao H. K., McCord T. B., and Nash D. B. (1973) Visible and near-infrared transmission and reflectance measurements of the Luna 20 soil. *Geochim. Cosmochim. Acta* **37,** 731–743.

Adams J. B. and McCord T. B. (1972) Electronic spectra of pyroxenes and interpretation of telescopic spectral reflectivity curves of the moon. *Proc. Lunar Sci. Conf. 3rd*, p. 3021–3034.

Bancroft G. M. and Burns R. G. (1967) Interpretation of the electronic spectra of pyroxenes. *Amer. Mineral.* **52,** 1278–1287.

Bell P. M. and Mao H. K. (1972) Crystal-field spectra of lunar samples. *Carnegie Inst. Wash. Yearb.* **71,** 479–489.

Bell P. M., Mao H. K., Hazen R. M., and Mao A. L. (1978)The Luna 24 sample from Mare Crisium: New structural features in lunar glasses deduced from a study of crystal-field spectra. In *Mare Crisium: The View from Luna 24* (R. B. Merrill and J. J. Papike eds.), p. 265–280. Pergamon, N.Y.

Burns R. G. (1970) *Mineralogical Applications of Crystal Field Theory*. Cambridge Univ. Press, Cambridge. 224 pp.

Burns R. G., Abu-Eid R. M., and Huggins F. E. (1972a) Crystal field spectra of lunar pyroxenes. *Proc. Lunar Sci. Conf. 3rd*, p. 533–543.

Burns R. G., Huggins F. E., and Abu-Eid R. M. (1972b) Polarized absorption spectra of single crystals of lunar pyroxenes and olivines. *The Moon* **4,** 93–102.

Burns R. G., Parkin K. M., Loeffler B. M., Leung I. S., and Abu-Eid R. M. (1976) Further characterization of spectral features attributable to titanium on the moon. *Proc. Lunar Sci. Conf. 7th*, p. 2561–2578.

Burns R. G. and Vaughan D. J. (1975) Polarized electronic spectra. In *Infrared and Raman Spectroscopy of Lunar and Terrestrial Minerals* (C. Karr, Jr., ed.), p. 39–72. Academic Press, N.Y.

Burns R. G., Vaughan D. J., Abu-Eid R. M., Witner M., and Morawski A. (1973) Spectral evidence for Cr^{3+}, Ti^{3+}, and Fe^{2+} rather than Cr^{2+} and Fe^{3+} in lunar ferromagnesian silicates. *Proc. Lunar Sci. Conf. 4th*, p. 983–994.

Charette M. P., Soderblom L. A., Adams J. B., Gaffey M. J., and McCord T. B. (1976) Age-color relationships in the lunar highlands. *Proc. Lunar Sci. Conf. 7th*, p. 2579–2592.

Charette M. P., Taylor S. R., Adams J. B., and McCord T. B. (1977) The detection of soils of Fra Mauro basalt and anorthositic gabbro composition in the lunar highland by remote spectral reflectance techniques. *Proc. Lunar Sci. Conf. 8th*, p. 1049–1061.

Cohen A. J. (1972) Trace ferric iron in lunar and meteoritic titanaugites. *The Moon* **4,** 141–154.

Goldman D. S. (1977) Crystal field and Mössbauer applications to the study of site distribution and electronic properties of ferrous iron in minerals with emphasis on calcic amphiboles, orthopyroxene and cordierite. Ph.D. Thesis, California Institute of Technology, Pasadena.

Goldman D. S. and Rossman G. R. (1977) The spectra of iron in orthopyroxene revisited: the splitting of the ground state. *Amer. Mineral.* **62,** 151–157.

Hazen R. M., Mao H. K., and Bell P. M. (1977) Effects of compositional variation on absorption spectra of lunar olivines. *Proc. Lunar Sci. Conf. 8th*, p. 1081–1090.

Loeffler B. M., Burns R. G., and Tossell J. A. (1975) Metal → metal charge transfer transitions: Interpretation of visible-region spectra of the moon and lunar materials. *Proc. Lunar Sci. Conf. 6th*, p. 2663–2676.

Loeffler B. M., Burns R. G., Tossell J. A., Vaughan D. J., and Johnson K. H. (1974) Charge transfer in lunar materials: Interpretations of ultraviolet-visible spectral properties of the moon. *Proc. Lunar Sci. Conf. 5th*, p. 3007–3016.

Manning P. G. (1968) Absorption spectra of the manganese-bearing chain silicates pyroxmangite, rhodonite, bustamite and serandite. *Can. Mineral.* **9,** 348–357.

Mao H. K. and Bell P. M. (1971) Crystal-field spectra. *Carnegie Inst. Wash. Yearb.* **70,** 207–215.

Mao H. K. and Bell P. M. (1973) Polarized crystal-field spectra of microparticles of the moon. *Amer. Soc. Test. Mater. Spec. Tech. Publ. 539*, 100–119.

Mao, H. K., Bell P. M., and Dickey J. S. (1972) Comparison of the crystal-field spectra of natural and synthetic chrome diopside. *Carnegie Inst. Wash. Yearb.* **71,** 538–541.

Rossman G. R. (1977) Optical absorption spectra of major minerals in Luna 24 sample 24170 (abstract). In *Papers Presented to the Conference. on Luna 24*, p. 156–159. The Lunar Science Institute, Houston.

Runciman W. A., Sengupta D., and Marshall M. (1973) The polarized spectra of iron in silicates. I. Enstatite. *Amer. Mineral.* **58,** 444–450.

Sung C.-M., Abu-Eid R. M., and Burns R. G. (1974) Ti^{3+}/Ti^{4+} ratios in lunar pyroxenes: Implications to depth of origin of mare basalt magma. *Proc. Lunar Sci. Conf. 5th*, p. 717–726.

Sung C.-M., Singer R. B., Parkin K. M., and Burns R. G. (1977) Temperature dependence of Fe^{2+} crystal-field spectra: Implications to mineralogical mapping of planetary surfaces. *Proc. Lunar Sci. Conf. 8th*, p. 1063–1079.